Study on the Preparation and Adsorption Property of Polyvinyl Alcohol/Cellulose Nanocrystal/Graphene Composite Aerogels (PCGAs)

Yan Wu[1,*], Xinyu Wu[1], Feng Yang[2,*], Li Xu[1] and Meng Sun[1]

[1]College of Furnishings and Industrial Design, Nanjing Forestry University, Nanjing, 210037, China.

[2]Fashion Accessory Art and Engineering College, Beijing Institute of Fashion Technology, Beijing, 100029, China.

[*]Corresponding Authors: Yan Wu. Email: wuyan@njfu.edu.cn; Feng Yang. Email: yangfeng@bift.edu.cn.

Abstract: The cellulose nanocrystals/graphene composite aerogel (CGA) and polyvinyl alcohol/cellulose nanocrystals/graphene composite aerogel (PCGA) were prepared by suspension titration, tert-butanol solution replacement and freeze-drying successively. The removal rates of methyl blue (MB) from water by CGA and PCGA were evaluated and the effects of additions, adsorption time, reaction temperature and pH value of CGA and PCGA on MB removal rate were discussed. It was found that the optimal concentrations of both CGA and PCGA were 2 g·L^{-1} in the adsorption reaction process and the adsorption equilibrium was reached within 120 min. The higher the initial pH value of MB solution is, the better the removal effect will be. The adsorption kinetics conformed to the pseudo-second-order kinetic model. The langmuir isothermal adsorption equation showed the maximum adsorption capacities of CGA and PCGA were 125 mg·g^{-1} and 110.9 mg·g^{-1}, respectively. Under the conditions of adsorption time of 120 min, reaction temperature of 323 K, and initial MB solution pH value of 11, both CGA and PCGA had higher removal rates of MB, reaching more than 98%.

Keywords: Cellulose nanocrystal; graphene; aerogel; adsorption

1 Introduction

With the continuous development of industry and agriculture, the environmental problems become more and more serious. In the dye industry, the pollution of waste water is the first problem. Due to the stable molecular structure of dye, it is difficult to remove from water. Moreover, it is highly toxic and teratogenic, posing a threat to biological health [1-4]. The spread of water pollution makes the removal of that becoming a research hotspot. Among them, the adsorption method has higher efficiency and lower cost, and its core lies in the production of adsorption materials with excellent functions. As a kind of light solid material with high porosity and specific surface area, aerogel has multiple active sites required by pollutant adsorption. Its strong adsorption capacity is also used in many fields such as water pollution control, sound insulation and noise reduction, and bio-medicine.

Cellulose nanocrystal (CNC) has been produced by using an acid hydrolysis approach from a range of cellulose sources. Disordered or paracrystalline regions of cellulose were preferentially hydrolyzed, whereas crystalline regions that have a higher resistance to acid attack remain intact [5]. It is generally between 100 nm and several micrometers in length, with small aspect ratio and large specific surface area [6-7]. Cellulose nanofibers are widely used in papermaking [8], pharmaceutical materials [9], composite materials [10] and other fields due to their good mechanical properties [11], ultra-fine structure [12], green and pollution-free characteristics [13], etc. Cellulose aerogel mainly consists of cellulose nanofibers with 3D porous framework and it has better ductility than ordinary inorganic aerogel (such as SiO$_2$ aerogel). Different cellulose materials and preparation methods will make the structure and properties of aerogel different. Hoepfner et al. [14] prepared cellulose aerogel through supercritical drying and freeze-drying

methods, respectively and the former having higher specific surface area but relatviely fragile. Wang et al. [15] first prepared translucent cellulose hydrogels by cellulose solvent and then high porosity cellulose aerogels was successfully obtained by solvent replacement. When cellulose aerogel is prepared by freeze-drying or supercritical carbon dioxide method, pore structure collapse can be avoided to a certain extent and it will have a great specific surface area and porosity.

In addition, introducing inorganic phase into aerogel system can improve its mechanical properties. Graphene (G) is rich in a variety of functional groups, with high specific surface area [16-17], super mechanical properties [18] and superconductivities [19-20]. The aerogel prepared from graphene also has a 3D porous structure, which makes graphene a promising catalytic and adsorption material [21]. Zheng et al. [22] used graphene oxide (GO) and carbon nanotubes to produce conductive aerogel with CNC, which can be used in the field of capacitors. The aerogel made by Bendahou et al. [23] through zeolite composite cellulose has excellent thermal insulation. Zhang et al. [24] prepared phthalic acid esters (PAE) resin crosslinked cellulose aerogel, which can quickly restore from the deformation. Zhao et al. [25] used polyethylenimine grafted CNC to prepare aerogel and the drug load and loading speed were significantly improved. Xiong et al. [26] made Ag adhere to cellulose aerogel and the aerogel had excellent antibacterial properties. Wan et al. [27] prepared super-hydrophobic and oil-absorbing cellulose aerogel which can be used in the field of oil adsorption.

Moreover, polyvinyl alcohol (PVA) has a feature of good water-soluble and compressive force, which is a kind of degradable organic matter of environmental protection. But its mechanics, heat resistance and water resistance are poor, resulting in its narrow application scope [28-29]. PVA and CNC have good hydrophilicity and they have complementary advantages in the mechanical strength. It was found that the mechanical strength and thermal stability of the composites obtained from the combination of CNC and PVA were significantly improved comparing with the pure CNC or PVA [30-31]. Wang et al. [32] produced the CNC/PVA composite films with the light transmittance of over 90%, high mechanical strength and ductility. Zhou et al. [33] prepared PVA/G composite films and found the tensile strength and elongation at break of the composite films were 1.4 and 1.7 times than that of pure PVA ones. Wang et al. [34] introduced CNC into PVA and used reduced graphene oxide (rGO) as the reinforcing phase. Biodegradable PVA/CNC/G composite films with excellent barrier and tensile properties were prepared by adding self-made CNC into PVA solution [35]. A large amount of hydroxyl groups on the surface of CNC can play a nano-strengthening role on PVA and improve the mechanical strength of PVA. PVA, CNC and G are compounded to produce composite aerogel (PCGA), which not only has the advantages of nano-materials, but also can strengthen the poor mechanical properties of aerogels, so that its application in catalysis, adsorption, heat preservation, energy storage and other aspects can be expanded.

CNC and graphene composites have a good adsorption performance, which is suitable for the treatment of dye waste. But normally, there is a strong interaction between the graphene layer and the solvent molecules, which is easy to lead to the collapses of the 3D porous structure of the aerogel [36]. This defect, to a large extent, affects the use efficiency of aerogel. PVA has a strengthening and stabilizing effect on GO aerogel, and the hydroxyl group on the surface of PVA can form a hydrogen bond structure with graphene, leading to an increase in mechanical strength [37-38].

Therefore, this paper started from the CNC and graphene which have excellent performance. The CNC was prepared through sulphuric acid hydrolysis then the graphene was added according to certain proportion. The cellulose nanocrystals/graphene composite aerogel (CGA) was prepared through ultrasonic mixing, suspended titration, alcohol solution displacement method and freeze drying, respectively. And then the CGA was characterized by using modern research methods and advanced equipments. The best ratio of graphene and CNC was selected according to the results of the characterization to prepare CGA samples for adsorption of methylene blue (MB) in water. Finally, the aerogel preparation technology was improved on the basis of the former optimal proportion. A certain proportion of PVA solution was added in the composite solution system of CNC and graphene, so that the polyvinyl alcohol/cellulose nanocrystals/graphene ternary composite aerogel (PCGA) was prepared. Finally, the structure and properties of PCGA were characterized by SEM, BET, XRD, FTIR, XPS and TG.

2 The Experimental Materials

The multilayer (around 10-50 layers) graphene-based carbon nanomaterial, a biomass-derived graphene product, was provided by the department of Sustainable Bioproducts, Mississippi State University (Mississippi, US). Kraft lignin (KL) supplied by Domtar Corp. (Plymouth, NC, USA) was used as a carbon source [39]. The experimental water was ultra-pure water from Nanjing Chemical Reagents Co. (Nanjing, China). Microcrystalline cellulose (column chromatography 97%) and methylene blue (analytical purity) were produced by Sinopharm Chemical Reagent Co., Ltd. (Nanjing, China). Anhydrous calcium chloride (analytical purity) was obtained from Shanghai Jiuyi Chemical Reagent Co., Ltd. (China). Concentrated sulfuric acid (98%), tert-butanol (analytical purity), sodium hydroxide (analytical purity), concentrated hydrochloric acid (analytical purity) and polyvinyl alcohol (type 1788) were purchased from Nanjing Chemical Reagent Co., Ltd. (China).

3 The Experimental Method

3.1 Preparation of PCGA

3.5 g PVA was weighed and poured into a triangle flask which contained 100 ml distilled water. The mixture was heated in the thermostatic magnetic stirrer until the solution was uniform and transparent without precipitation. According to m (CNC): m (PVA) = 1:1, the CNC suspenstion and PVA solution both with the concentration of 3.5 wt% were weighed as 10 g, respectively. Then according to a ratio of m (CNC + PVA): m (G) = 100:1, graphene powder was added into the PVA/CNC solution. Then the ultrasonication was used to mix the PVA/CNC/G solution with 80% power ultrasound for 20 min in ice-water bath. Next, the PVA/CNC/G solution was extracted with a 5 ml syringe, and then slowly dropped into the standard $CaCl_2$ solution with a concentration of 0.25 mol/L by suspension titration. The solution was then allowed to stand for more than 24 hours until the gel was formed stably. The prepared PVA/CNC/G composite gels were sequentially placed in tert-butanol solutions with concentrations of 30%, 60% and 100%, respectively. The above three concentrations were replaced for 24 hours each, and changed every 12 hours. After the tert-butyl alcohol solvent fully replaced the water in PVA/CNC/G wet gels, which were put into the freezing dryer at -40°C for 36 hours, the PCGAs were obtained.

3.2 The Characterization of CGA and PCGA

(1) The morphology observation

The tweezer was used to fix CGA and PCGA on the sample holder by conductive adhesive. Attention should be paid to keep the structure and morphology of the aerogels intact. Then the sample surface was sprayed by gold for 30 seconds and the scanning electron microscope (SEM, FEI Quanta 200, USA) was used to observe the surface and internal morphologies of CGA and PCGA at the voltage of 3 kV. The solutions for preparing CGA and PCGA were observed by transmission electron microscopy (TEM, JEM-1400, Japan). Before testing the solutions were diluted by 1000 times and stirred by ultrasound for 10 minutes.

(2) BET test

About 100 mg of the above prepared CGA and PCGA were weighed and placed in the degassing tube. After degassing, the nitrogen adsorption-desorption test was performed by using the automatic surface area and aperture distributor (ASAP2020 HD88, Micromeritics, USA).

(3) X-ray diffraction (XRD) test

The CGA and PCGA were grounded into fine powders, and they were as fine and uniform as possible. Appropriate amount of powder was spread in the sample tank and the powder was overspread evenly. XRD (Ultima IV, RIgaku) was used to characterize the molecular structure of CGA and PCGA. The voltage was 40 kV, the range was $2\theta = 5° - 60°$ and the scanning speed was 10 °/min.

(4) Fourier transform infrared spectrometer (FTIR) test

The surface functional groups of the prepared CGA and PCGA were measured by FTIR (VERTEX 80V, Bruker, USA). The CGA and PCGA were fully dried for backup and compressed with KBr to

determine the spectrum. The wave number range was 4000-500 cm^{-1}.

(5) X-ray photoelectron spectroscopy (XPS) test

The qualitative and quantitative analysis of the surface elements of CGA and PCGA were finished by XPS (AXIS UltraDLD, Shimadzu, Japan). The CGA and PCGA were pressed into sheets with a tablet press and fixed on the double-sided adhesive tape. XPS spectral analysis was carried out in the mode of constant energy analyzer. The CGA and PCGA were scanned in full spectrum and the individual elements were analyzed within the range of 0-1200 eV.

(6) TG test

The thermogravimetric analyzer (TG209F3, NETZSCH, German) was used to test thermal degradation properties of CGA and PCGA. The heating rate was kept 10 ºC/min and the temperature range was 30-500ºC.

3.3 Adsorption Experiment of Methylene Blue in Water by CGA and PCGA

The methylene blue (MB) solution was equipped at the concentration of 1.0 g/L and reserved at 4ºC in the refrigerator. The MB solution was diluted to 0.1, 0.25, 0.5, 1, 2.5, 5 and 10 mg/L, respectively.

4 Results and Discussion

4.1 Characterization Test Analysis

4.1.1 Morphology Analysis

It could be observed from Fig. 1 that the CGA (a, b) and PCGA (c, d) had the typical interconnected three-dimensional network structures, showing porosity, disorder and uneven network surface. The same structure and similar pore structure indicated that PVA did not destroy the skeleton of CGA, which was consistent with Wang and Li [40]. However, the pore size distribution of the two type aerogels was different. Observation from the magnification (Figs. 1(b) and 1(d)), the spatial stereoscopic effect of CGA was stronger and the average pore size was much larger than that of PCGA.
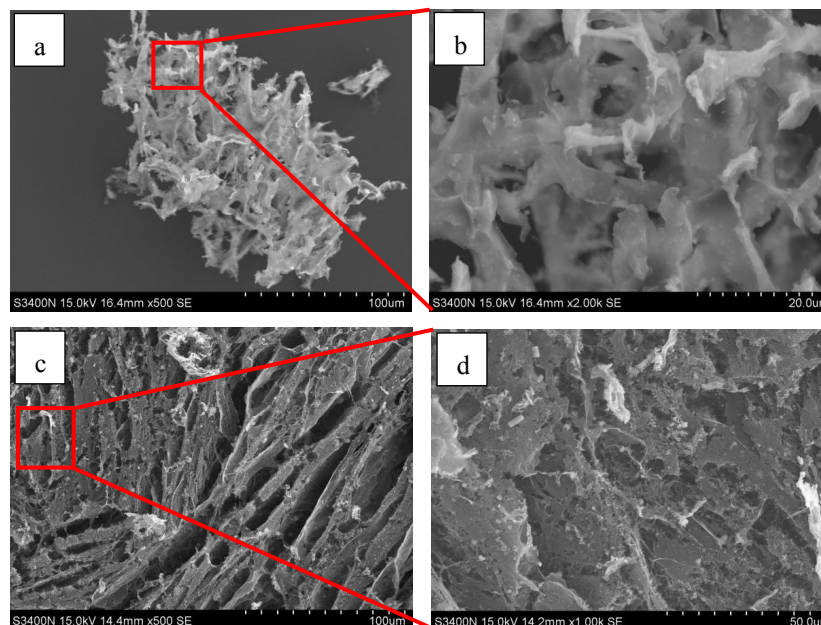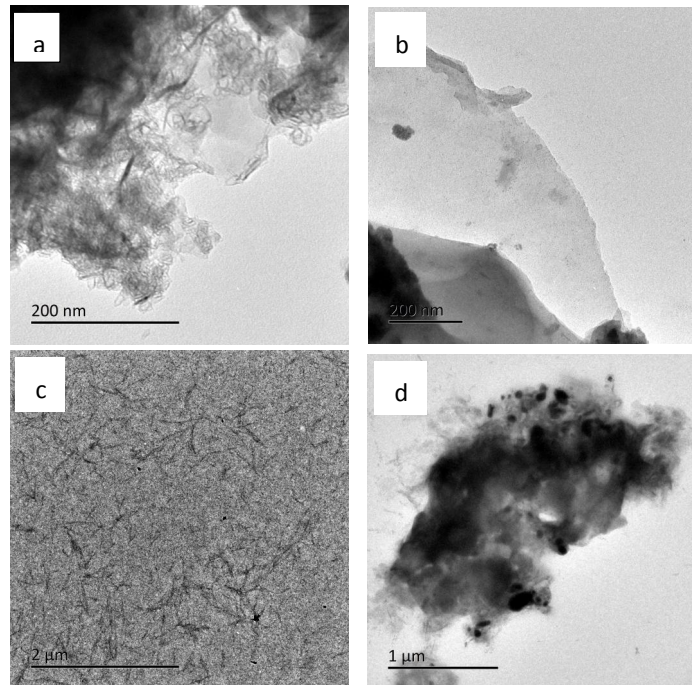

Figure 1: SEM images of CGA (a, b) and PCGA (c, d)

Fig. 1(b), the average pore size of CGA was more than 5 μm, mostly large holes. While the pore size of PCGA was within 1~2 μm (Fig. 1(d)), mostly mesopores and micropores. Moreover, the CGA structure

was more uniform while the PCGA showed a richer and heavier layered structure, which might be the addition of PVA cause it to combine with CNC and G, producing more crosslinked molecules and forming a more compact structure.

TEM was used to further confirm the accumulation situation of the microstructure of PCGA composite aerogel after the above PVA was added. The solutions for preparing CGA and PCGA could be observed in Fig. 2. The graphene showed the tortuous and granular sheet-like (Figs. 2(a) and 2(b)) and CNCs were in the form of short rods (Fig. 2(c)). The solution for making CGA could be seen uniformly dispersing in a large amount of rod CNCs and graphene firmly fixed on the surface of the CNCs. While the image of solution for making PCGA (Fig. 2(d)) showed a misty structure, indicating that the PVA polymer has been well blended with G and CNC, however, there was also a sign of local agglomeration. The FTIR spectrum in Fig. 5 also showed that there was a strong interaction between the PVA layer, the graphene sheet and CNC, resulting in the more stable and uniform structure of PCGA.

Figure 2: TEM images of graphene (a, b), solutions for making CGA (c) and PCGA (d)

4.1.2 BET Analysis

As was seen from Fig. 3 that the adsorption isotherms of CGA and PCGA belonged to the IV type in the IUPAC classification and the H3 adsorption isotherm with the retention loop. The sudden increases of nitrogen adsorption at the high-pressure end indicated the existence of mesopores and macropores on the CGA and PCGA surfaces, which was the result of multi-layer adsorption on the solid uniform surfaces. The addition of PVA led to a decrease in the specific surface area of PCGA, which might be due to the fact that PVA caused local agglomeration more severely. The PVA itself was a crystalline polymer with good film-forming property. The addition of PVA increased the solution viscosity, compacted the aerogel surface and decreased the pore size structure of PCGA, which were consistent with the results of SEM analysis.
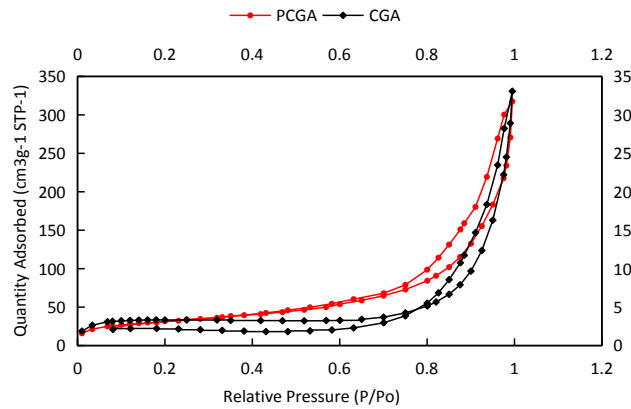
**Figure 3:** N$_2$ adsorption-desorption diagrams of CGA and PCGA

4.1.3 XRD Analysis

It could be observed from XRD diagrams (Fig. 4) that the diffraction peaks of 14.6° (101 crystal plane), 16.5° (10$\bar{1}$ crystal plane) and 22.7° (002 crystal plane) were strong peaks which were closed to typical characteristic peaks of cellulose I type structure. And the diffraction peak of 22.4° was the characteristic of graphene. It indicated that the crystal structure of CNC and graphene remained intact after PVA was added. The addition of PVA increased the crystallinity of PCGA to 79.6% and the intensity of the diffraction peak of CGA was higher than that of PCGA.
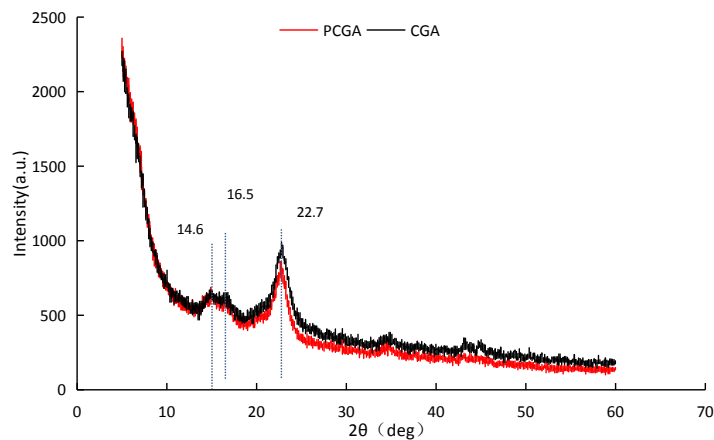
Figure 4: XRD diagrams of CGA and PCGA
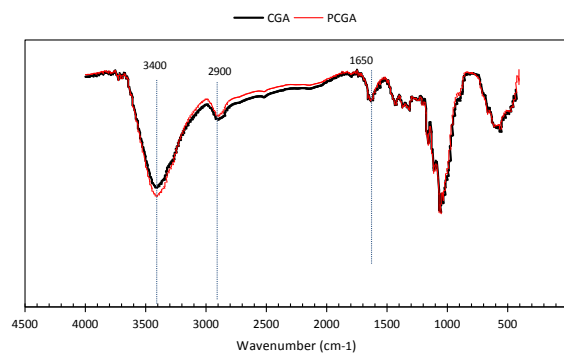
Figure 5: FTIR diagrams of CGA and PCGA
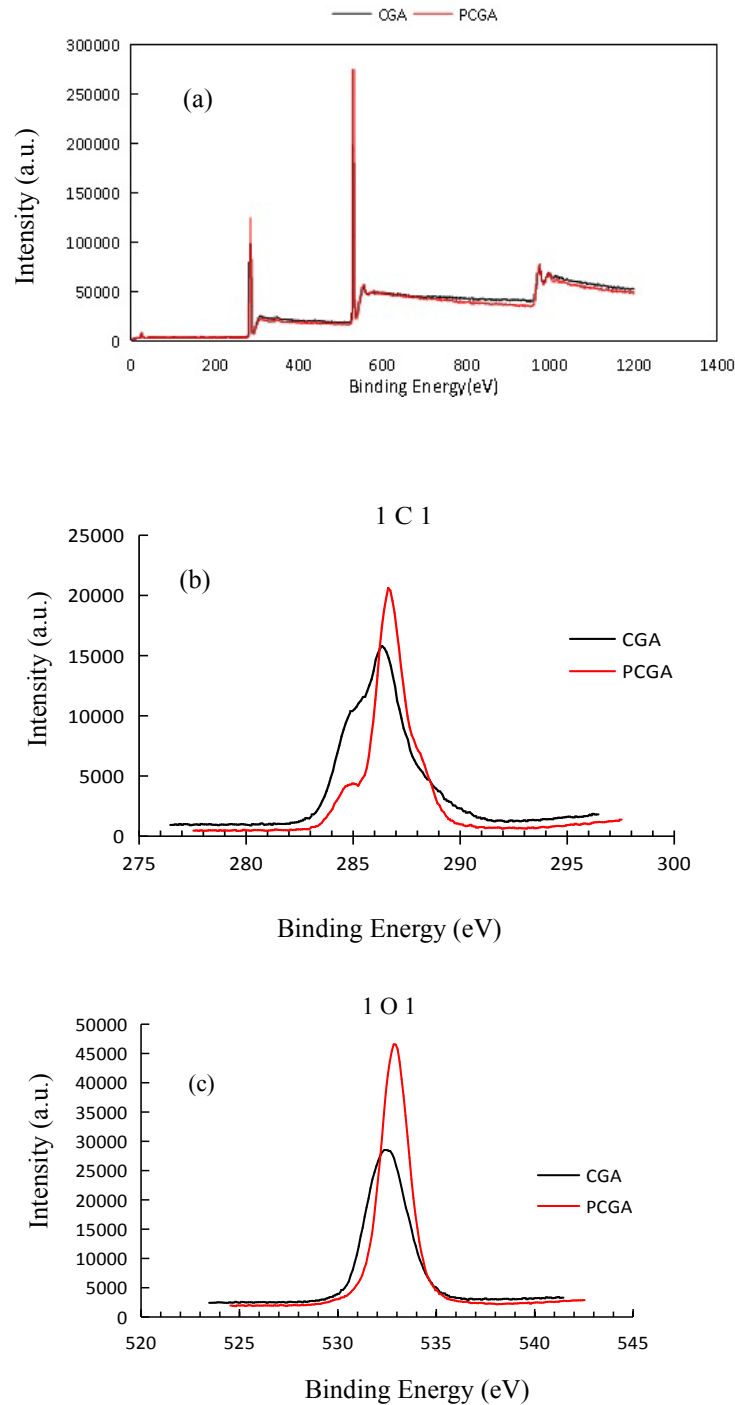
Figure 6: XPS diagrams of CGA and PCGA

4.1.4 FTIR Test

The vibration absorption peaks near 3400 cm^{-1} corresponded to the stretching vibration of -OH, 2900 cm^{-1} corresponded to the stretching vibration of -CH$_2$, the vibration absorption peaks at 1650 cm^{-1} and 1375 cm^{-1} were the stretching vibration and bending vibration of -COOH in cellulose, respectively. The PVA matrix had only a weak effect on the stretching strength of CNC at -OH, which might be due to the cross-linking of -OH on the surface of CNC and adjacent -OH in PVA, but the binding of -OH on PVA itself was

not affected. Therefore, the combination of CNC and PVA was physical rather than chemical. This indicated that the type of functional groups in the composite aerogel prepared with PVA was not changed and a large number of hydroxyl groups and carboxyl groups remained.

4.1.5 XPS Analysis

The O1s peak (532 eV) and C1s peak (286 eV) were the main peaks as shown in the high-resolution XPS spectra (Fig. 6), indicating that the addition of PVA had no significant influence on CGA. It could be found that the C/O of CGA was 2.0, while the C/O of PCGA was reduced to 1.54, indicating that the oxidation degree of PCGA was higher than that of CGA. The C1s and O1s peaks of PCGA at 286 eV and 532 eV were both significantly stronger than that of CGA, which indicated the increase of carbon and oxygen contents in PCGA and the addition of PVA improved the composite aerogel structure.

4.1.6 TG Analysis

It could be seen from Fig. 7(a) that the first stage of weight loss in CGA and PCGA was both in the temperature range from ambient to 150°C, which was mainly caused by water evaporation. The second major stage of weight loss (240 - 350°C) was the thermal degradation of the main chain of CNC. At the beginning of each heating stage, the thermal weight loss and weight loss rate of CGA and PCGA were smaller and the initial decomposition temperature was at 240°C.

The maximum thermal decomposition rate of PCGA was at about 300°C, which was 10°C lower than the CGA one as shown in Fig. 7(b). This might be due to the addition of PVA in PCGA, which resulted in the reaction between PVA and CNC consuming more hydroxyl groups on the cellulose chain and hindering the formation of intermolecular hydrogen bonds in the regeneration process, thus reducing the thermal stability of PCGA.
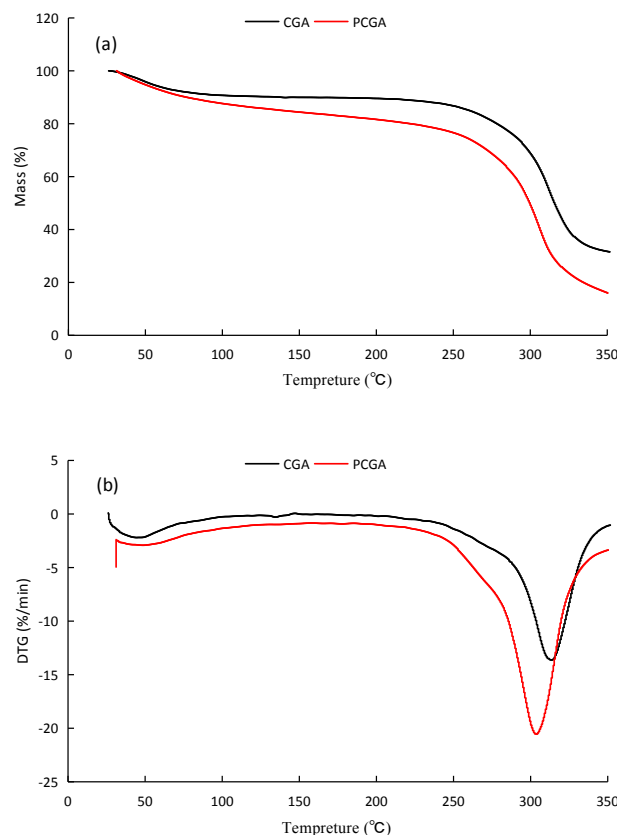

**Figure 7:** TG (a) and DTG (b) diagrams of CGA and PCGA

4.2 Adsorption of Methyl Blue in Water by CGA and PCGA

The light adsorption value of MB solution was measured by ultraviolet spectrophotometer (PerkinElmer LAMBDA 1050 UV/vis/NIR spectrophotometer) in 200-800 nm. The light absorbance at 664 nm was recorded and the standard curve of MB solution was drawn and fitted. The X axis (C) represents the concentration of MB solution and Y axis (A) represents the light absorbance and the standard equation $A = 0.2035 \times C + 0.0012$ was obtained. As was shown in Fig. 8, the removal rate of MB first increased and then decreased with the addition of CGA and PCGA. When the addition of aerogels was from 2 mg to 10 mg, the removal rate of MB increased and the removal effect was significantly enhanced. When the addtion was beyond 20 mg, the removal rate of MB was basically stable and slightly decreased. The highest value was 94.7% with 20 mg PCGA added, which was slightly lower than that in CGA (96.0%/20 mg). The adsorption amount first increased and then decreased mainly because of the increase of CGA and PCGA at the beginning, the adsorbent specific surface area and adsorbable sites increased. As the contents of CGA and PCGA continued to increase, the adsorbents of each unit were able to absorb less MB.
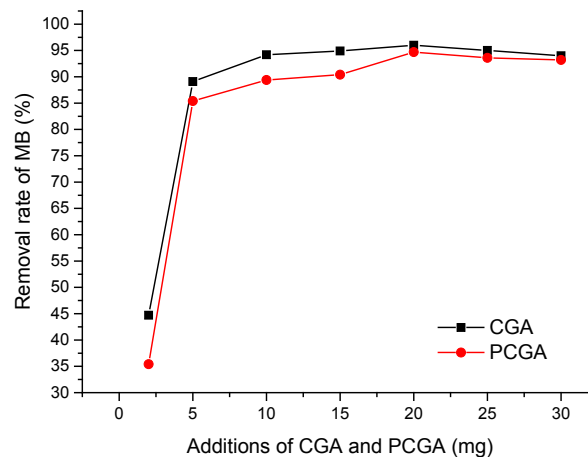
Figure 8: Effect of additions of CGA and PCGA on the removal rate of MB
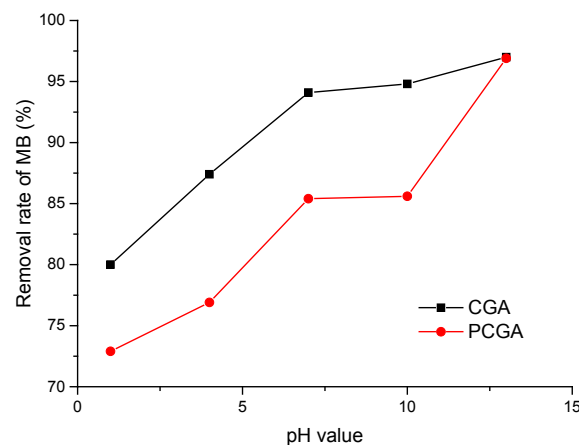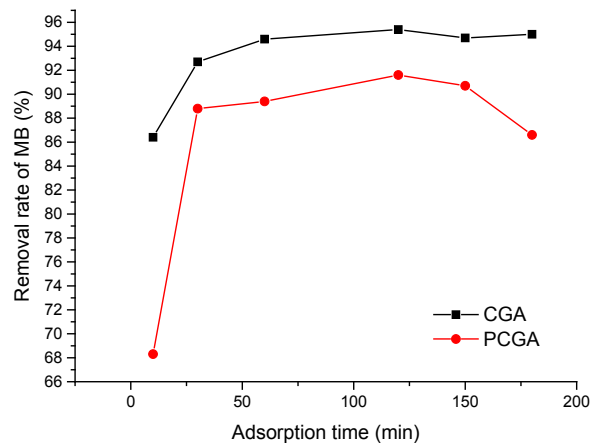

Figure 9: Effect of pH value on the removal rate of MB

It could be clearly seen from Fig. 9 that with the pH value increased from 1 to 13 and the initial concentration of MB solution was 100 mg·L^{-1}, the removal rate of MB in CGA and PCGA showed an increasing trend. When the pH value of MB solution was 1, CGA and PCGA had the lowest removal rate of MB (80.0% and 72.9%), respectively. When the pH value was low, the positive charge of a large amount of H^+ in the strong acid solution was consistent with the one on the surface of MB, resulting in competitive adsorption. When the pH value was 13, the removal rate of MB was up to the highest value in CGA and

PCGA, which was 97.0%, indicating that the alkaline condition was conducive to the adsorption of aerogels.

As was shown in Fig. 10, the removal rate of MB by CGA and PCGA first increased and then tended to slightly slow down with increasing adsorption time. At first 30 min, the reaction rate was very fast. When the adsorption time was from 30 min to 120 min, the removal rate of MB by CGA and PCGA reached maximum values of 95.4% and 91.6%, respectively. And the removal rate of MB became slightly lower at the adsorption time of 150 min and 180 min, which perharps because after a large amount of MB was adsorbed, the difference in the concentration of MB between the two phases decreased, the remaining MB in the solution had a weaker driving force toward the aerogel adsorption site.


Figure 10: Effect of adsorption time of CGA and PCGA on the removal rate of MB

As was shown in Fig. 11, with the increase of temperature and initial MB solution concentration, the adsorption capacity of PCGA increased. This might because the number of collisions between PCGA and MB was one of the decisive conditions affecting the adsorption rate. As the temperature increased, PCGA produced new adsorption sites, which promoted the internal diffusion transmission rate of MB into PCGA. Therefore, the higher the temperature and initial MB solution concentration were, the more favorable PCGA adsorption of MB was, indicating that the adsorption process was endothermic.
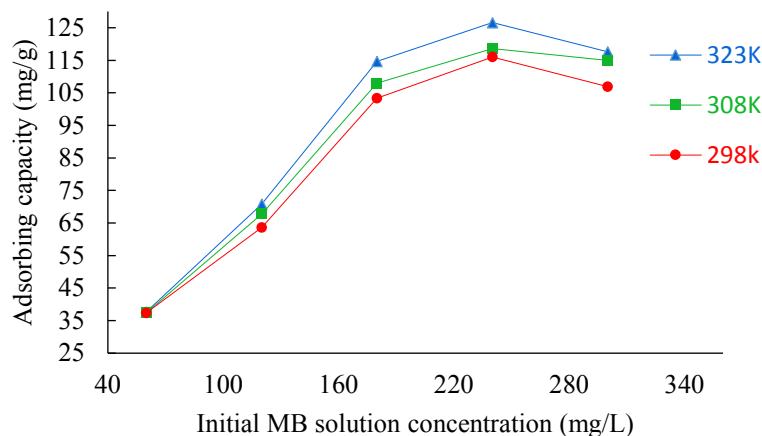
Figure 11: Effect of initial MB solution concentration on the adsorbing capacity of PCGA at different temperatures

The adsorption isotherms of MB removal by PCGA referred to equations that $c_e/q_e = c_e/q_{max} + 1/q_{max} \cdot k_L$ and $R_L = 1/(1 + k_L \cdot_c 0)$, the Langmuir equation for removal of MB was fitted and the following Fig. 12(a) was obtained. Where, c_e is the equilibrium adsorption concentration ($mg \cdot L^{-1}$), q_e is the equilibrium adsorption quantity ($mg \cdot g^{-1}$), q_{max} is the maximum adsorption quantity ($mg \cdot g^{-1}$), k_L is the adsorption constant ($L \cdot mg^{-1}$), c_0 is the maximum value ($mg \cdot L^{-1}$) in different initial mass concentrations of the dye solution. If $0 < R_L < 1$, the adsorption process is favorable; if $R_L > 1$, the adsorption process is adverse adsorption; if $R_L = 1$, it is linear adsorption; if $R_L = 0$, it is an irreversible adsorption.
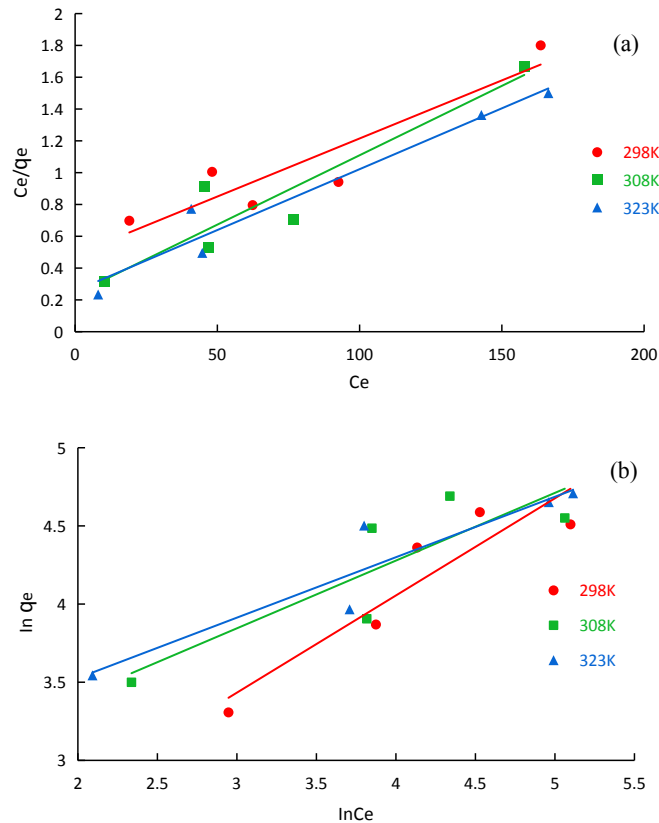
**Figure 12:** Langmuir (a) and Freundlich (b) equation fitting curves for removal of MB by PCGA

Table 1: Fitting parameters of Langmuir and Freundlich equations for removal of methylene blue (MB) by PCGA

temperature	Langmuir equation			Freundlich equation		
	q_{max} /$mg \cdot g^{-1}$	k_L /$L \cdot g$	R^2	$1/n$	k_F	R^2
298 K	98.3	0.020	0.847	0.622	4.479	0.858
308 K	108.9	0.039	0.874	0.433	12.745	0.736
323 K	110.9	0.035	0.949	0.387	15.690	0.873

In addition, the Freundlich equation can be used to describe the adsorbent with uneven surface. The equation for removal of MB by PCGA was fitted according to formula $\ln_{q_e} = \ln_{k_F} + 1/n \cdot \ln_{c_e}$, and the fitting curves and parameters were shown in Fig. 12(b) and Tab. 1, respectively. Where, c_e is the equilibrium adsorption concentration ($mg \cdot L^{-1}$), q_e is the equilibrium adsorption quantity ($mg \cdot g^{-1}$), and K_F is a constant related to the adsorption capacity, representing whether the adsorption performance is good or not. N is a constant related to the adsorption strength. If $n < 1$, it means that adsorption is difficult; if $1 < n < 2$,

adsorption is hard; if 2 < n < 10, the adsorption strength is large and the adsorption is easy.

It was found from Fig. 12 that the linear of Langmuir equation was better than Freundlich equation. The values of q_{max} acquired from Langmuir equation were 98.3 mg·g⁻¹, 108.9 mg·g⁻¹ and 110.9 mg·g⁻¹ at different temperatures, respectively. They were closer to the maximum adsorption capacity obtained experimentally and comparable of the previous studies for various adsorbents, such as multiwall carbon nanotube (335.7 mg·g⁻¹) [41], discarded tyres activated carbon (137.1 mg·g⁻¹) [42], peanut husk (51.02 mg·g⁻¹) [43] and corn stalk cellulose (9.06 mg·g⁻¹) [44]. From Tab. 1, it was calculated that the R^2 value of Langmuir equation was better than that of Freundlich equation, indicating that Langmuir model was more suitble for the thermodynamic process of the adsorption of MB by PCGA. It could be concluded from table 1 that 1/n values at different temperatures (298 K, 308 K, 323 K) were all less than 1, indicating that PCGA was feasible and easy to remove methylene blue from water.
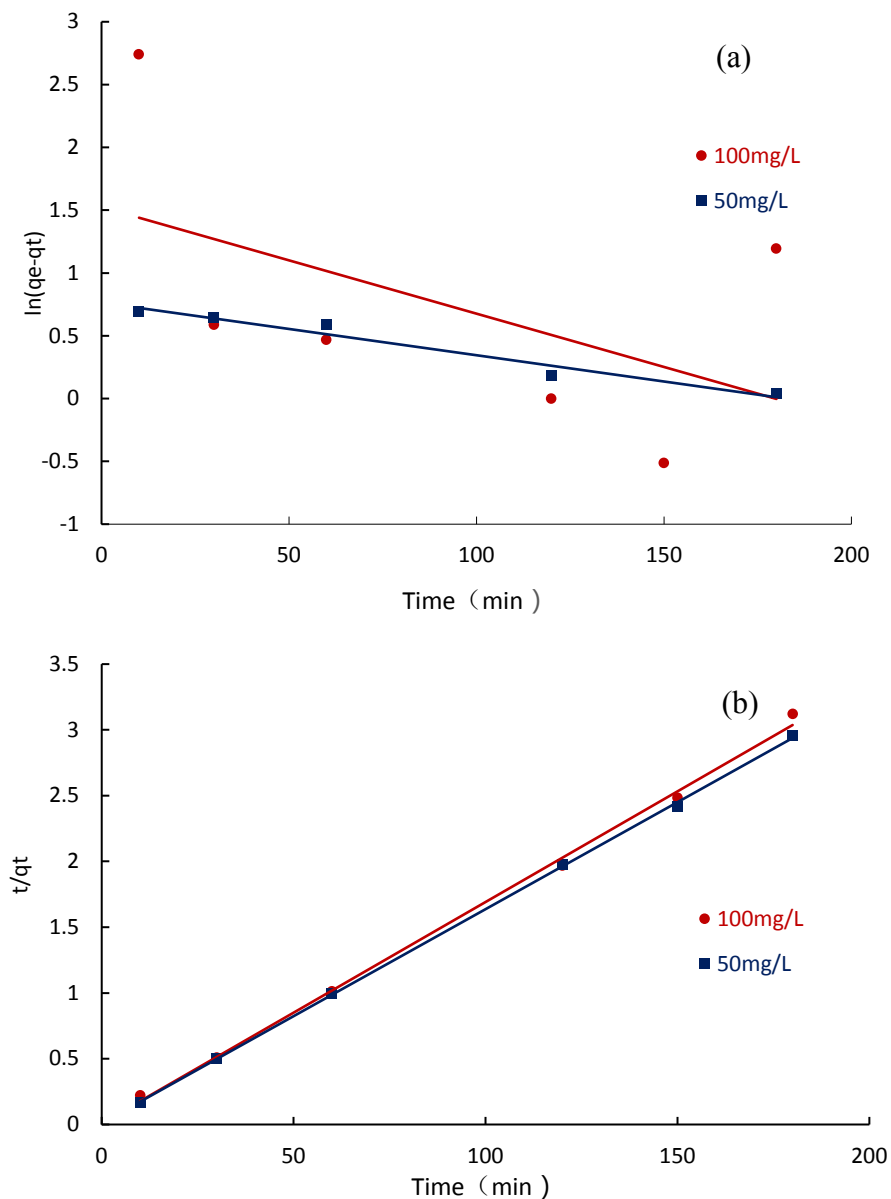
Figure 13: Pseudo-first-order (a) and pseudo-second-order (b) kinetic fitting curves for MB removal by PCGA

It was found from Fig. 13 that the Pseudo-second-order kinetic model (Fig. 13(b)) was more suitable for the dynamic adsorption analysis of MB removal by PCGA than the Pseudo-first-order kinetic model (Fig. 13(a)). Tab. 2 summarized the kinetic equation fitting parameters and R_2^2 was better than R_1^2, R_1^2 was further from 1, $q_{e,1}$ was far less than $q_{e,2}$, so PCGA adsorption kinetics of MB was suitable for pseudo-secondary kinetic model. The adsorption was slow and the equilibrium time was long, indicating that the adsorption of MB by PCGA was chemical adsorption.

Table 2: Pseudo-first-order and pseudo-second-order kinetic equation fitting parameters for MB removal by PCGA

Concentration $mg \cdot L^{-1}$	Pseudo-first-order kinetic equation fitting parameters			Pseudo-second-order kinetic equation fitting parameters		
	$q_{e,1}/mg \cdot g^{-1}$	k_1	R_1^2	$q_{e,2}/mg \cdot g^{-1}$	k_2	R_2^2
100	4.314	0.009	0.266	59.524	0.030	0.998
50	2.111	0.004	0.930	61.350	0.025	0.999

5 Summary

PCGA was successfully prepared by freeze-drying with a compounding of 3.5 wt % CNC suspention, 3.5 wt % PVA solution and biomass graphene at a ratio of m (CNC): m (PVA): m (G) = 100:100:1. With the help of SEM, TEM, BET, XRD, FTIR, XPS, TGA, PCGA was characterized and compared with CGA. The comprehensive performance of PCGA was better. The pore size of PCGA surface with the addition of PVA became smaller and the local agglomeration led to the decrease of specific surface area. The addition of PVA increased the crystallinity and decreased the thermal stability of PCGA than CGA. The reaction between PVA and CNC consumed more hydroxyl groups on the cellulose chain, which hindered the formation of intermolecular hydrogen bonds in the regeneration process. Under the conditions of adsorption time of 120 min, reaction temperature of 323 K, initial MB solution pH value of 11, initial MB concentration of 100 mg·L^{-1}, and PCGA addition of 20 mg, the removal rate of MB by PCGA reached up to the ultimate value, which was more than 98%. The thermodynamic process of the adsorption of MB by PCGA was fitted well to the Langmuir model.

References

1. Zeng, W. (2017). *Modified graphene oxide material preparation and its adsorption properties of methylene blue in waste water*. Hunan University, Hunan.

2. Birhanli, A., Ozmen, M. (2005). Evaluation of the toxicity and teratogenity of six commercial textile dyes using the frog embryo teratogenesis assay-xenopus. *Drug and Chemical Toxicology, 28(1),* 51-65.

3. Huang, C., Dong, H., Su, Y., Wu, Y., Narron, R. et al. (2019b). Synthesis of carbon quantum dot nanoparticles derived from byproducts in bio-refinery process for cell imaging and *in vivo* bioimaging. *Nanomaterials, 9(3),* 387.

4. Huang, C., Lin, W., Lai, C., Li, X., Jin, Y. et al. (2019c). Coupling the post-extraction process to remove residual lignin and alter the recalcitrant structures for improving the enzymatic digestibility of acid-pretreated bamboo residues. *Bioresource Technology,* 121355.

5. Chen, W., Yu, H., Lee, S. Y., Wei, T., Li, J. et al. (2018). Nanocellulose. a promising nanomaterial for advanced electrochemical energy storage. *Chemical Society Reviews, 47,* 2837-2872.

6. Elazzouzi, H. S., Nishiyama, Y., Putaux, J., Heux, L., Dubreuil, F. et al. (2008). The shape and size distribution

of crystalline nanoparticles prepared by acid hydrolysis of native cellulose. *Biomacromolecules, 9(1),* 57.

7. Rahimi, M., Behrooz, R. (2011). Effect of cellulose characteristic and hydrolyze Conditions on morphology and size of nanocrystal cellulose extracted from wheat straw. *International Journal of Polymeric Materials & Polymeric Biomaterials, 60(8),* 529-541.

8. Huang, C., Chu, Q., Xie, Y., Jin, Y., Min, D. et al. (2015). Effect of kraft pulping pretreatment on the chemical composition, enzymatic digestibility, and sugar release of moso bamboo residues. *Bioresources, 10,* 240-255.

9. Huang, C., Sun, R., Chang, H., Yong, Q., Jameel, H. et al. (2019a). Production of dissolving grade pulp from tobacco stalk by SO$_2$-ethanol-water (SEW), alkaline extraction and bleaching processes. *Bioresources, 14(3),* 5544-5558.

10. Wu, Y., Wang, S., Zhou, D., Zhang, Y., Wang, X. et al. (2013). Biodegradable polyvinyl alcohol nanocomposites made from rice straw fibrils. Mechanical and thermal properties. *Journal of Composite Materials, 47(12),* 1449-1459.

11. Yan, X., Qian, X., Lu, R., Miyakoshi, T. (2019). Synergistic effect of addition of fillers on properties of interior waterborne UV-curing wood coatings. *Coatings, 8(1),* 9.

12. Sun, T. (2016). *Preparation and characterization of nanocellulose hybrid aerogel*. Shandong Agricultural University.

13. Xu, W., Wu, Z., Zhang, J. (2014). Effects of species and growth ring angles on acoustic performance of wood as resonance boards. *Wood and Fiber Science, 46(3),* 412-420.

14. Hoepfner, S., Ratke, L., Milow, B. (2008). Synthesis and characterisation of nanofibrillar cellulose aerogels. *Cellulose, 15(1),* 121-129.

15. Wang, Z., Liu, S., Matsumoto, Y., Kuga, S. (2012). Cellulose gel and aerogel from Li Cl/DMSO solution. *Cellulose, 19(2),* 393-399.

16. Wang, Y., Zeng, L. (2015). Research progress of graphene/epoxy resin composites. *Adhesion, 4,* 87-91.

17. Xiong, X., Bao, Y., Liu, H., Zhu, Q., Lu, R. et al. (2019). Study on mechanical and electrical properties of cellulose nanofibrils/graphene-modified natural rubber. *Materials Chemistry and Physics, 223(2),* 535-541.

18. Lan, Y. (2014). Overview of research progress of graphene. *Development Direction of Building Materials, 5,* 46-46.

19. Chu, Y., Liu, J., Fang, Q., Jiang, L. (2009). Carbon material graphene and its application in electrochemical capacitors. *Battery, 4,* 200-201.

20. Balandin, A. A., Ghosh, S., Bao, W., Calizo, I., Teweldebrhan, D. et al. (2008). Superior thermal conductivity of single-layer graphene. *Nano Letters, 8,* 902-907.

21. Ren, L., Hui, K. N., Hui, K. S., Liu, Y., Qi, X. et al. (2015). 3D hierarchical porous graphene aerogel with tunable meso-pores on graphene nanosheets for high-performance energy storage. *Scientific Reports, 5,* 14229.

22. Zheng, Q., Javadi, A., Sabo, R., Cai, Z., Gong, S. (2013). Polyvinyl alcohol (PVA)-cellulose nanofibril (CNF)-multiwalled carbon nanotube (MWCNT) hybrid organic aerogels with superior mechanical properties. *RSC Advances, 3(43),* 20816-20823.

23. Bendahou, D., Bendahou, A., Seantier, B., Grohens, Y., Kaddami, H. (2015). Nano-fibrillated cellulose-zeolites based newhybrid composites aerogels with super thermal insulating properties. *Industrial Crops and Products, 65,* 374-382.

24. Zhang, W., Zhang, Y., Lu, C., Deng, Y. (2012). Aerogels from crosslinked cellulose nano/micro-fibrils andtheir fast shape recovery property in water. *Journal of Materials Chemistry, 22(23),* 11642-11650.

25. Zhao, J., Lu, C., He, X., Zhang, X., Zhang, W. et al. (2015). Polyethyleneimine-grafted cellulose nanofibril aerogels as versatile vehicles for drug delivery. *ACS Appl Mater Interfaces, 7(4),* 2607-2617.

26. Xiong, R., Lu, C., Wang, Y., Zhou, Z., Zhang, X. (2013). Nanofibrillated cellulose as the support and reductant for the facile synthesis of Fe$_3$O$_4$/Ag nanocomposites with catalytic and antibacterial activity. *Journal of Materials Chemistry A, 1(47),* 14910-14918.

27. Wan, C., Lu, Y., Sun, Q., Li, J. (2014). Preparation and characterization of novel lignocellulose aerogel with hydrophobicity and oil absorption properties. *Science and Technology Guide, 32(1),* 79-85.

28. Zhang, F. (2017). *Synthesis of functional cellulose nanofibril aerogels and their applications*. Nanjing Forestry University, Nanjing.

29. Wang, X., Li, Y., Lian, H., Chen, Y., Guo, L. et al. (2018). Preparation and properties of functional graphene/polyvinyl alcohol composite films, *Chinese Journal of Forestry Engineering, 3(2),* 109-115.

30. Cho, M. J., Park, B. D. (2011). Tensile and thermal properties of nanocellulose reinforced poly (vinyl alcohol)

nanocomposites. *Journal of Industrial and Engineering Chemistry, 17(1),* 36.

31. Popescu, M. C., Dogaru, B. I., Goanta, M., Timpu, D. (2018). Structural and morphological evaluation of CNC reinforced PVA/starch biodegradable films. *International Journal of Biological Macromolecules, 116,* 385-393.

32. Wang, Z., Jiang, J., Si, Y., Fan, Y. (2017). Effect of cellulose nanofibers on the property of cellulose nanofiber/polyvinyl alcohol composite film. *Chinese Journal of Papermaking, 32(40),* 27-31.

33. Zhou, T., Chen, F., Tang, C., Bai, H., Zhang, Q. et al. (2011). The preparation of high performance and conductive poly (vinyl alcohol)/graphene nano-composite via reducing graphite oxide with sodium hydrosulfite. *Composite Science Technology, 71(9),* 1266-1270.

34. Wang, X., Guo, L., Feng, Q., Wei, J., Shi, L. et al. (2008). Preparation and properties of polyvinyl alcohol/cellulose nanofiber/graphene composite films, *Chinese Journal of Forestry Engineering, 3(5),* 84-90.

35. Lin, F., Lu, Q., Huang, B., Tang, L. (2018). Research progress of nanocellulose and its polymer nanocomposites, *Chemical Engineering Progress, 37(5),* 3454-3470.

36. Lin, D., Chen, G., Fang, Z. (2017). Preparation and properties of NFC composite aerogel supercapacitors. *Paper Science & Technology, 36(1),* 28-35.

37. Wu, Y., Tang, Q., Yang, F, Xu, L., Wang, X. et al. (2019). Mechanical and thermal properties of rice straw cellulose nanofibrils-enhanced polyvinyl alcohol films using freezingand-thawing cycle method. *Cellulose, 26(5),* 3193-3204.

38. Ha, H., Shanmuganathan, K., Ellison, C. J. (2015). Mechanically stable thermally crosslinked poly (acrylic acid)/reduced graphene oxide aerogels. *ACS Applied Materials & Interfaces, 7(11),* 6220-6229.

39. Zhang, X., Yan, Q., Li, J., Chu, I., Toghiani, H. et al. (2018). Carbon-based nanomaterials from biopolymer lignin via catalytic thermal treatment at 700 to 1000ºC. *Polymers, 10,* 183.

40. Wang, H., Li, D. (2014). Investigation on PVA/cellulose nanofibers composites with three-dimensional network. *Plastics Industry, 42(4),* 116-119.

41. Adebayo, M. A., Porla, L. D., Lima, E. C., Puchana-Rosero, M. J., Cataluña, R. et al. (2014). Adsorption of Procion Blue MX-R dye from aqueous solutions by lignin chemically modified with aluminium and manganese. *Journal of Hazardous Materials, 268,* 43-50.

42. Rozada, F., Otero, M., García, A. I., Morán, A. (2007). Application in fixed-bed systems of adsorbents obtained from discarded tyres and sewage sludge. *Dyes and Pigments, 72,* 47-56.

43. Noreen, S., Bhatti, H. N., Nausheen, S., Sadaf, M., Ashfaq, M. (2013). Batch and fixed bed adsorption study for the removal of Drimarine Black CL-B dye from aqueous solution using a lignocellulosic waste. A cost affective adsorbent. *Industrial Crops and Products, 50,* 568-579.

44. Wu, L., Sun, J., Wu, M. (2017). Modified cellulose membrane prepared from corn stalk for adsorption of methyl blue. *Cellulose, 24,* 5625-5638.